43rd AIAA Aerospace Sciences Meeting and Exhibit, 10-13 Jan 2005, Reno, Nevada

Hydrodynamic Model of Plasma-Sheath for RF Discharges with and without Collision

Haribalan Kumar* and Subrata Roy†

Computational Plasma Dynamics Laboratory, Kettering University, Flint, Michigan 48504

We present a numerical model for two-species bounded plasma discharge with a time varying potential at 0.1 torr pressure in collisional and collisionless regimes. The plasma-wall problem is modeled using hydrodynamic equations coupled with the Poisson equation. The model is based on a robust finite element algorithm utilized to overcome the stiffness of the plasma-wall equations. Appropriate flux boundary conditions with directions are imposed at both electrodes. Typical discharge characteristics including electron gas flooding at electrode, sheath heating, sheath evolution with time and electric double layer are predicted. The spatial and temporal evolution of charge density, electric field and total current are documented. Numerical limitations are also highlighted from the theoretical derivation of algorithm amplification factor and phase velocity.

Nomenclature

x (z)	Spatial co-ordinate, cm
t (τ)	Time co-ordinate, s
n (N)**	Number density, cm^{-3}
V (u)	Species velocity, cm/s
S	Ionization frequency, s^{-1}
Γ	Flux, cm^{-2}/s
p	Pressure, torr
μ	Mobility, $cm^2V^{-1}s^{-1}$
D	Diffusion coefficient, cm^2/s
$\Re$	Speed of ionization, cm/s
T	Temperature, eV
E	Electric field, V/cm
e	Electron charge, statcoulomb
φ (ϕ)	Potential, V
I	Current, Amp/cm^2
ε	Permittivity
d	Characteristic length, cm
C	Capacitance, farad
λ_{De}	Electron Debye length, cm
λ_i	Ion mean free path, cm
ω	Applied frequency, radians
Ω	Computational domain
Δ	Increment
F	Solution Residual
G^h	Amplification factor
Φ^h	Relative phase velocity

** Terms appearing within braces are normalized variables

Subscripts:

γ	Species
e	Electron

* Graduate Research Assistant, kuma6164@kettering.edu. 1700 West Third Ave, and AIAA Student Member.

† Associate Professor of Mechanical Engineering, sroy@kettering.edu. 1700 West Third Ave, AIAA Associate Fellow.

i Ion
B Bohm
0 Reference value

I. Introduction

THE usage of direct current (DC) and radio frequency (RF) driven discharges in many fields including material processing, microelectronics and aerospace industry necessitates development of effective numerical predictive tools to understand and design their behavior. The theoretical prediction of DC discharges based on experimental data was reported as early as 1962.[1] These discharges are characterized by continuous steady currents and are mostly sustained by secondary emissions. However, the load factor (ratio of electric field to Lorentz force) for DC sheath application is of the order 1, far from the Stoletow point, thus unsuitable for ionization purposes. A popular alternative method is through the application of unsteady RF fields with frequencies in range of 1 to 100 MHz. Understanding RF induced sheath dynamics near the surface of an electrode has a strong effect on both volume ionization efficiency and on energy interactions with the neutral gas flow.[2,3] Specifically, with the recent progress in RF plasma-based boundary layer flow control[3-5], where the fundamental mechanisms remain unclear, the understanding of RF plasma and its bounding sheath has become crucial. This requires a theoretical modeling technique that is geometry versatile and time accurate. Here, we attempt to model bounded plasma up to and including the sheath near the electrodes at 0.1 torr pressure.

At low discharge pressures (~millitorr) applicable to the semiconductor and material processing industries, the dynamics of RF sheath has been studied by early researchers.[6-8] There are a few methods for modeling plasma-wall under applied RF potential. These include the bulk plasma model, the step-front-electron sheath model, and the asymptotic expansion method. Godyak and Sternberg[9] have modeled the sheath of a symmetric RF discharge in the frequency range $\omega_{pi} << \omega_{rf} << \omega_{pe}$ for varying degrees of collision and sheath voltages. Slemrod[10] models two fluid plasma using asymptotic expansions. The dynamics of plasma due to external RF current is determined separately in the bulk, transition and sheath regions. Nitschke and Graves[11] have compared the PIC and fluid models for RF discharge of helium gas for a range of pressure (50mTorr-250mTorr) and electrode gap (40mm to 120mm).

These theoretical advances notwithstanding, a self-consistent simulation for RF driven plasma-wall interactions remains a quest. In a self-consistent plasma-wall model, the space charge effect is incorporated for the entire discharge. Recently, two such plasma-wall models have been reported for two component fully ionized plasma[12] and three component partially ionized gas.[3] The two fluid model was applied to predict the RF discharge inside a tube filled with argon gas. The three fluid model characterized the effect of volume ionization on the neutral helium gas flow between two dielectric coated electrodes at atmospheric pressure. The intention is to complement experimental efforts by providing a suitable tool to explore flow control concepts in future design and development.

Following Roy *et al.*[12], here we present a detailed comparative study of the space charge effect in a two-fluid capacitive RF plasma-wall system in the presence and absence of collisional impact ionization. A high-fidelity finite-element procedure anchored in the Multiscale Ionized Gas (MIG) flow code[3,12-14] is implemented to model the argon gas between a RF powered and a grounded electrode. The basic hydrodynamic equations are formulated using a finite element algorithm to overcome the numerical stiffness issues. This paper is organized as follows. Section II describes the problem specifications. Section III specifies the boundary conditions and the normalization schemes adopted. Section IV explains the methodology used to solve the system of equations. Section V describes and interprets the computed results. Section VI summarizes the conclusions.

II. Problem Statement

Fig. 1 shows the circuit for a typical capacitive RF discharge. A time varying potential is applied at the right electrode through a blocking capacitor C. The left electrode is grounded. We consider two-fluid plasma consisting of electrons and ions. The unsteady continuity and momentum (drift-diffusion) equations are solved simultaneously with the Poisson equation. The transverse extent of the discharge is assumed to be much larger than the inter-electrode distance and hence a one-dimensional model is considered sufficient. When the ion mfp is comparable or less than maximum sheath width, ions involve in more than one ionizing collisions. Thus, the argon plasma at 0.1 torr is collisional. However, to identify the effects of collision in the space-charge separated sheath region, we consider the problem first without the collision and then with the collisional effects. Hereafter we will refer to Case A for collisionless sheath model, while Case B represents the collisional sheath model. The ionization is present in the bulk plasma in both cases.

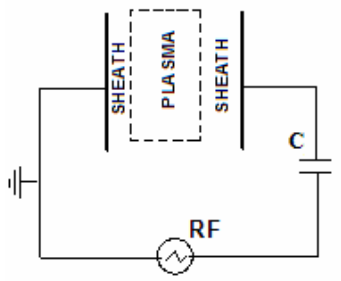

Figure 1: Schematic of the capacitive RF discharge

The following fluid equations are used. The continuity equation for electron (e) and ion (i) number densities is,

$$\frac{\partial n_g}{\partial t} + \frac{\partial \Gamma_g}{\partial x} = n_e S \text{ , for species } g = e, i \tag{1}$$

where, n_g is the species density, V_g is the species hydrodynamic velocity. A collisionless condition (zero ionization) is ensured inside the sheath in case A. For case B, the ionization frequency is governed by the Townsend equation

$$S = Ae^{-B/(E/p)^{0.4}} p\Re \tag{2}$$

where A and B are known for the gas[15]. We introduce the *speed of ionization* $\Re = m_e E$ (which has a dimension of velocity, cm/s) to model the spatially and temporally varying ionization.

The electrons flux is governed by

$$\Gamma_e = -n_e m_e E - D_e \frac{\partial n_e}{\partial x} \text{ with } D_e = m_e T_e/e. \tag{3}$$

The electron mobility m_e is given by[1] $pm_e = 3\times10^5 cm^2 V^{-1} s^{-1} Torr$, at p=0.1 Torr. The electron temperature (T_e) is 1 eV. For ions, in case A, the inertial term is included in the formulation of its momentum,

$$\frac{\partial V_i}{\partial t} + V_i \frac{\partial V_i}{\partial x} = \frac{e}{m} E - g_i V_i \tag{4}$$

While for case B, the flux can be derived from the drift velocity and hence,

$$\Gamma_i = n_i m_i E - D_i \frac{\partial n_i}{\partial x} \tag{5}$$

Here electric field E=-$\partial j/\partial x$. For cold ions at T_i = 0.025 eV, $D_i = 2\times10^2$ cm^2/s. The ion mobility m_i is based on the degree of ionization, electric field and pressure.[1] The following Poisson equation is used to calculate the potential drop.

$$\frac{\partial^2 j}{\partial x^2} = -\frac{e}{e}(n_i - n_e) \tag{6}$$

Inserting Eq. (1) into (6) and integrating on x gives the following current balance,

$$e\frac{\partial^2 j}{\partial x \partial t} = e n_i V_i - e n_e V_e + I(t) \tag{7}$$

where the constant of integration, $I(t)$, is the total current density. It may be noted that the effect of varying speed of ionization on the rate of species production is indirectly reflected on the net current density as can be seen from Eq. (7).

The sheath edge is identified as the ion attains the modified Bohm velocity based on Godyak-Sternberg[9] (G-S) as $V_B[1+c]^{-0.5}$ where the collision parameter $c = 0.5p\, l_{De} / l_i$ and λ_i(cm)[16] ~1/330p.

III. Boundary Conditions

The left electrode is grounded, $j(0)$= 0, and a sinusoidal RF potential $j_{rf} = j_{rms}\sin 2pft$ with j_{rms}=100V and f=13.56 MHz is applied to the right electrode through the capacitor (C = 0.1) where $\partial j(2)/\partial t = I(t)/\mathrm{C}$, and j may be related to total current through Eqn. (7) thereby completing the circuit in Fig. 1.

The electron flux at both electrodes is based on the electron thermal velocity ($V_{e,th}$) whose magnitude is given by $G_e = n_e V_{e,th}/4$ and is directed towards the wall. For case A, we utilize the collisionless model and employ Boltzmanian electron distribution at the wall. Hence the flux becomes,

$$\Gamma_e = n_e\sqrt{\frac{T_e}{2p\,m_e}} = n_e^{|z_w-\Delta z|}\sqrt{\frac{T_e}{2p\,m_e}}e^{-\Delta f}$$

Homogeneous Neumann boundary condition ($\partial n_i/\partial x=0$) is imposed for ions at both electrodes.

The system of equations (1)-(7) is normalized using the domain length (d) and applied frequency (f) as fundamental quantities:

$t = 2p\,ft$, $z=x/d$, $N_g = n_g/n_0$, $u_g = V_g/V_B$ for $g=e, i$

and $f = ej/T_e$, $S = Sd/V_B$ where the Bohm velocity $V_B = \sqrt{T_e/m_i}$ and the reference density $n_0=10^{10}$ cm^{-3}.

IV. Methodology

The ionized argon gas is numerically modeled using the finite-element based Multiscale Ionized Gas (MIG) flow code. The code is modular and separate subroutines can be written to model different physics. Here, the equation sets (1) and (6) can be written with operator L as L (**q**) = 0 where **q** = $\{N_i, N_e, f\}^T$ is the state variable. Multiplying with a permissible test function y and integrating over the spatially discretized domain Ω, the variational statement results in the weak form

$$WS^h = \Im_e\left(\int_{\Omega_e}[y\,L(\mathbf{q})dt\,]\right)_e = 0$$

for a discretization h of $\Omega = \bigcup\Omega_e$ and $\Im_e$ is the non-overlapping sum over the elements. Thus the GWS form of Eq. (1) becomes,

$$\sum_e\left(\int_{\Omega_e} y\,y^T dz\left(\frac{d\{N_g\}_e}{dt}\right)+\left\{\int_{\partial\Omega_e} y\,(\Gamma_g)^T dz\{N_g\}_e - \int_{\Omega_e}\frac{dy}{dz}(\Gamma_g)^T dz\{N_g\}_e\right\} - S\int_{\Omega_e} y\,y^T dz\{N_e\}_e\right)_e = F_g \tag{8}$$

where F_g is the solution residual, and the GWS form of Eq. (2) with residual F_f is

$$\sum_e\left(-\int_{\partial\Omega_e} y\,\frac{dy^T}{dz}dz\{f\}_e + \int_{\Omega_e}\frac{dy}{dz}\frac{dy^T}{dz}dz\{f\}_e + \int_{\Omega_e} y\,y^T dz\{N_e\}_e - \int_{\Omega_e} y\,y^T dz\{N_i\}_e\right)_e = F_f \tag{9}$$

The domain is discretized into 400 elements and y is interpolated using a linear basis function. The Jacobian matrix $J=[\partial F/\partial\mathbf{q}]$ in $[J].\{\partial\mathbf{q}\} = -\{F\}$ is resolved using LU-decomposition scheme for updating change in discretized solution vector **q** at each iteration. The terminal non-linear ordinary differential equation (ODE) systems derived from Eqs. (8)-(9) are solved using implicit Euler method for temporal evolution and N-R iterative algorithm for the non-linear matrix algebra. We used the convergence criterion for all variables at any iteration as 10^{-3}.

The stability of the above algorithm can be investigated from its amplification factor G^h and the relative phase velocity Φ^h. For example, based on the finite element stencil for Eq. (8), using Fourier representation, one may derive the following amplification factor for ions,

$$G^h = \left[1-3iCf(m\Delta z)-S\Delta t(\cos q + i\sin q)\right]^{-1} \tag{10}$$

with the magnitude $\left|G^h\right| = \left((1-S\Delta t\cos q)^2 + (3Cf(m\Delta z)+S\Delta t\sin q)^2\right)^{-0.5}$

and the phase velocity $\Phi^h = \tan^{-1}\left[\frac{(3Cf(m\Delta z)+S\Delta t\sin q)}{(1-S\Delta t\cos q)}\right]\Big/ -Cm\Delta z$, (11)

while those for electrons are:

$$G^h = \left[1-3iCf(m\Delta z)-S\Delta t\right]^{-1}$$
$$\left|G^h\right| = \left[(1-S\Delta t)^2 + (3Cf(m\Delta z))^2\right]^{-0.5} \tag{12}$$

and $\Phi^h = \tan^{-1}\left[\frac{3Cf(m\Delta z)}{(1-S\Delta t)}\right]\Big/ -Cm\Delta z$. (13)

Above m is the wave number, Δz is the length of an element, C is the Courant number, $f(m\Delta z) = \sin m\Delta z/(2+\cos m\Delta z)$ and $q = -(u_e^h - u_i^h)m(n+1)\Delta t$ is the relative velocity phase angle. Here, we have analyzed for $\theta = 0$, which includes both ions and electrons. The algorithm is stable if $|G^h|\le 1$. One prefers $\Phi^h \sim 1$ to minimize the loss of information during solution process. Figure 2 plots $|G^h|$ as a function of $m\Delta z$ for two values of S

and C. Obviously for higher value of ionization rate S_2 = 500, the solution becomes unstable. The numerical difficulty may be handled by appropriate selection of Courant number and introduction of artificial diffusion. The result however gives an insight to the increasing instability of the standard solution procedure about the bulk-sheath transition region.

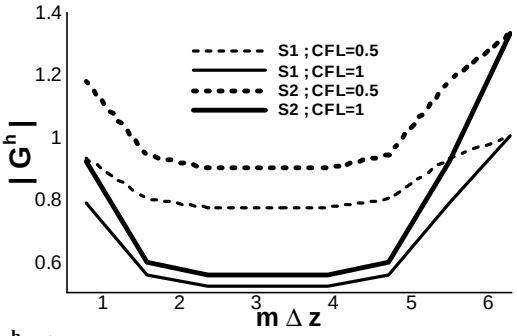

Figure 2: Amplification factor ($|G^h|$) for varying Courant numbers (C=0.5 and 1) and ionization rates S1 = 5 and S2 = 500.

V. Results and Discussion

Case A:

Figure 3 shows the computed RF discharge characteristics for a collisionless sheath at applied frequency $w << w_{pe}$. The discharge gets established due to external power supply in form of a sinusoidal wave at the right electrode. The inherent difference between ion and electron inertia is one fundamental concept, governing the discharge. The direction and magnitude of the electric field is based on the space charge separation. The spatio-temporal evolution of ϕ and E in Fig. 3(a) and Fig. 3(b) match well with those published in literature[16, 17]. It is interesting to note that the slope of *E* is always positive for most of the simulation domain and near the powered electrode the magnitude always remains positive. This indicates the DC bias of the potential. Fig. 3(c) gives an approximate indication of sheath edge location at which space charge separation become prominent as the ion and electron density curves bifurcate. But for the local RF oscillations in the sheath, this trend is representative of a typical DC sheath under collisionless conditions[3].

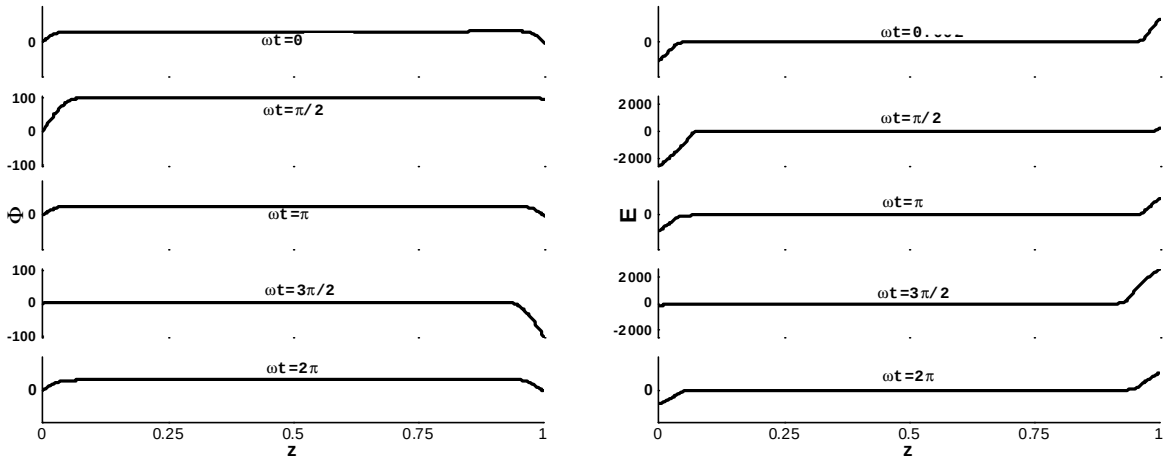

(a) (b)

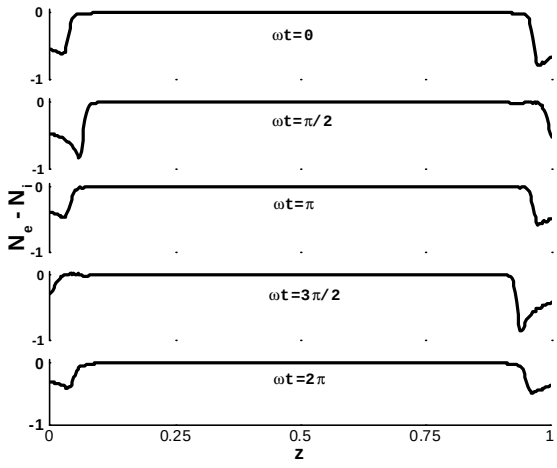

(c)

Figure 3: Variation of (a) Potential, (b) Electric field and (c) Charge separation at various instants of the RF cycle

Case B:

Figures 4-7 illustrate the computed RF discharge characteristics for the collisional model. The time-averaged values of potential and electric field for one RF cycle are shown in Fig 4. The average potential of one cycle has been compared to the potential in Fig 4(a) when it reaches its maximum value at $\pi/2$. The average discharge potential is ~40% of the peak potential. Also notice that plasma potential (in the bulk) is always positive and vanishes to zero potential at the electrodes. Hence this also explains the positive nature of the space charge sheath formed. The time-averaged electric field in the domain for one RF cycle is shown in Fig 4(b). In the bulk plasma, the field cancels out in opposing half of applied potential and hence there is not net force on the charged particles. The direction of the field, as mentioned before is always pointed towards the electrode.

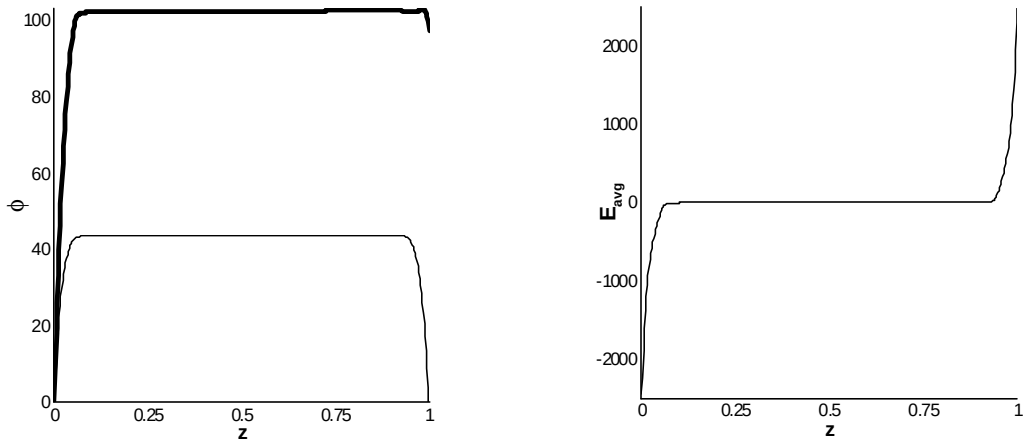

(a) (b)

Figure 4: (a) Time averaged (thin line) and peak potential at p/2 (thick line) and (b) Time averaged electric field.

The flooding and receding of the electron gas, exposing the immobile ions to the electrode (periodically) at every *kp* radians is shown in Figure 5(a). There is an increase of electron density at the electrode momentarily collapsing the electron sheath, which is otherwise inevitable. This energy is imparted to the electrons through accelerating fields. The electrons thus oscillate about the center of the domain driven by the potential difference across the electrodes.

Figure 5(b) shows the extent of deviation of plasma from quasi-neutrality in the presence of electrodes. Unlike case A, there is no clear sheath edge boundary due to the presence of collisions. The magnitude of charge separation is greater in case B than in case A also attributed to the ionization in the sheath. The spatial evolution of net charge in the domain differs between cases A and B, particularly in the plasma-sheath edge. For example, as we move from the bulk plasma to sheath, there is a sharp drop in electron density (due to high cathode potential) and the sheath is almost devoid of electrons near grounded electrode at $\pi/2$. In case A, ions are collisionless inside the sheath; and to preserve the flux, they gradually decay to a non-zero value. In case B, ions experience more than one ionizing collisions inside sheath.

The profiles of potential and electric fields for collisional discharge are similar to case A except for higher magnitudes of E induced in the sheath for case B. The electric field in the bulk plasma is observed to be a periodic function in the timescale of the applied frequency as $E(\tau) \sim 3\cos(\pi+\tau)$. A close look at the sheath edge near the powered electrode, however, demonstrates the formation of an electric double layer[11] in Fig. 5(c). The phenomenon is noticeable near an electrode in the positive half of applied potential (see at $\pi/2$) and occurs at relatively weak electric fields. Ions, due to their high inertia, hardly respond to the weak fields in the bulk plasma. This is not true in sheath. The highly oscillating fields exert high electrostatic force on the ions and they enter the sheath with high velocities. The timescales of ions and applied frequency are comparable for this plasma density and plasma frequency.

Fig 5(d) shows the electron heating ($G(\tau).\mathbf{E}(\tau)$) profile. It is evident that electrons are periodically heated and cooled corresponding to the sheath oscillation and hence the electron energy increases or decreases accordingly. The effect of electrical double layer amplifying the electron heating near sheath edge (similar to the effect on flux as mentioned above) is also noticed. Sheath heating is a dominant phenomenon in radio frequency driven discharges.

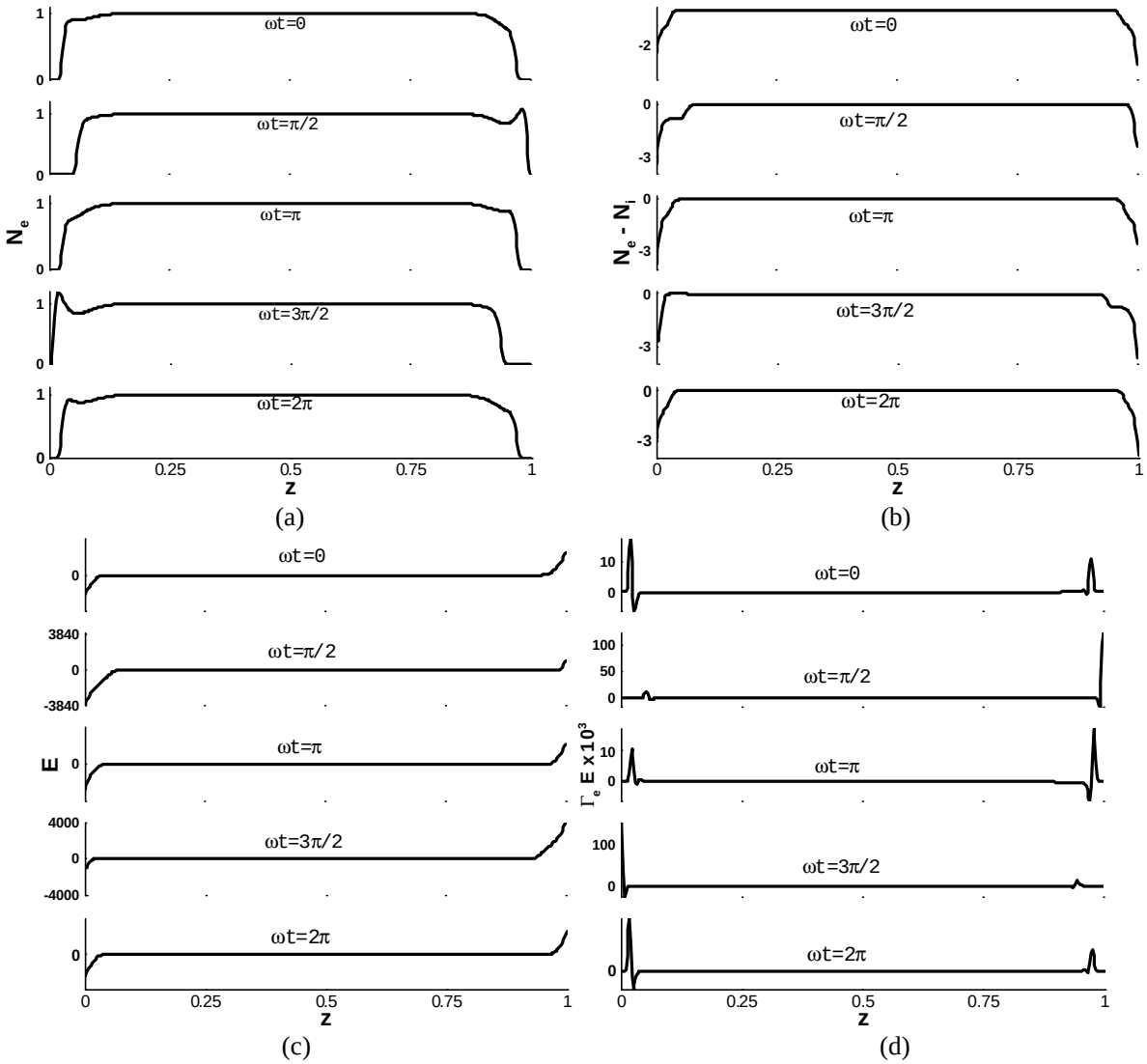

Figure 5: Variation of (a) the Electron Number density, (b) the Charge separation, (c) the Electric field, and (d) the Electron heating at various time stations of the RF cycle.

The electron flux in the bulk is estimated to vary as $N_e u_e \sim 28\cos\tau$. Electrons, being lighter get transported across the domain in reponse to the applied potential. Due to their high mobility, the effect of double layer is amplified causing a local fluctuation near the sheath edge (e. g at $\pi/2$) which gets reflected $N_e u_e$ causing a local fluctuation as seen in Fig 6(a). The variation of total current at the powered electrode for 3 cycles of applied potential is reported in Fig. 6(b). The total current is conserved in space at any particular moment. It should be noted that the displacement current and conduction (electron and ion) current magnitudes are comparable at the subject pressure of 0.1 torr. The peak of the

total current is observed at every $(4k+1)\pi/2$. A minor secondary peak is also observed in Fig. 6(b) at the instant when the applied potential switches direction on the electrode. We also note that this secondary current peak is less significant for lower ionization rates.

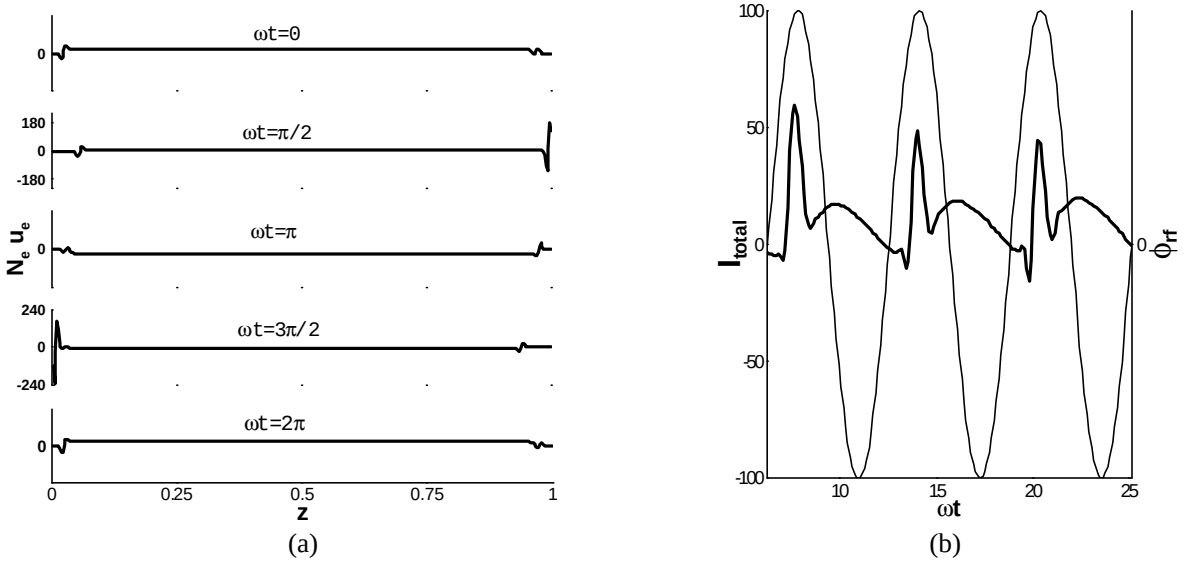

(a) (b)

Figure 6: (a) Spatio-temporal variation of Electron flux and (b) Temporal evolution of wall potential (thin solid line) and total current (dark solid line)

The difference in normalized sheath thickness at the grounded left electrode (z_L) and the powered right electrode ($1-z_R$) shows an expected 2π periodicity between the points of extremum sheath locations with a phase lag of π radians. The oscillation of sheath width z_w is plotted in Fig. 7 using the G-S relation stated in Sec. II. Based on curve fitting with an estimation error of ~4%, we correlate the sheath thickness as $z_w \approx 0.04 \pm 0.03 \sin t$. For the discharge at 0.1 torr, the simulation results predict the maximum sheath width $z_{w\text{-}max} \sim 20\ l_{De}$, which agrees with the available literature[16]. The sheath accounts for nearly 80 % potential drop for one RF cycle. The average sheath thickness was numerically found to be higher for a collisionless sheath under similar conditions than a collisional one.

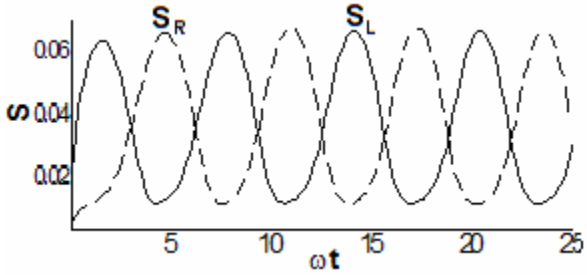

Figure 7: Temporal evolution of Left ($S_w=z_L$) and right ($S_w=1-z_R$) sheath width

VI. Conclusions

An argon gas discharge between two electrodes under collisionless and collisional regimes has been modeled from first principles using a self-consistent system of two fluid and a single Poisson equations. The dynamics of ions and electrons have been reported for applied RF potential with frequency $\omega << \omega_{pe}$ and 0.1 torr pressure. The results of collisionless discharge matches well with literature. The coupled nature of the problem, varying timescales for charged species in the bulk plasma and sheath, and the use of an interpolation polynomial to simulate the plasma-sheath transition that has abrupt changes in gradients add to the complexity of the problem. The periodic interaction of the electron gas with the electrode and local fluctuations in the form of electric double layers at weak fields are predicted near instantaneous anodes. A DC-bias of the potential field is also documented. The oscillation of the sheath edge has been correlated as a sinusoidal wave. The sheath is of few Debye lengths and accounts for nearly 80% potential drop for one RF cycle. The versatile finite element algorithm employed here will be extended to higher-dimensional discharge configurations and to high-pressure (barrier) discharges in the future.

Acknowledgements

This work was partially supported by the Air Force Research Laboratory contract no. F33615-98-D-3210. The first author gratefully acknowledges many helpful discussions with Prof. Natalia Sternberg and Dr. Datta Gaitonde for modeling the discharge.

References

[1]L. Ward, Journal of Applied Physics, 33(9), 2789 (1962).
[2]I. V. Adamovich, V. V. Subramaniam, J. W. Rich and S. O. Macheret, AIAA Journal, 36, 816 (1998).
[3]S. Roy and D. Gaitonde, Journal of Applied Physics, 96(5), 2476 (2004).
[4]J. R. Roth, Physics of Plasmas, 10(5), 2117 (2003).
[5]C. L. Enloe, T. E. Mclaughlin, R. D. VanDyken, et al., AIAA Journal, 42(3), 595 (2004).
[6]P. A. Miller and M. E. Riley, Journal of Applied Physics, 82(8), 3689 (1997).
[7]D. Bose, T. R. Govindan and M. Meyyappan, Journal of Applied Physics, 87(10), 7176 (2000).
[8]Y. Zhang, J. Liu, Y. Liu and X. Wang, Physics of Plasmas, 11(8), 3840 (2004).
[9]V. A. Godyak and N. Sternberg, Physical Review A, 42(4), 2299 (1990).
[10]M. Slemrod, SIAM Journal of Applied Math., 63(5), 1737 (2003).
[11]T. E. Nitschke and D. B. Graves, Journal of Applied Physics, 76(10), 5646 (1994).
[12]S. Roy, B. P. Pandey, J. Poggie and D. Gaitonde, Physics of Plasmas, 10(6), 2578 (2003).
[13]S. M. Cooper, B. A. Cruden, M. Meyyappan, R. Raju and S. Roy, Nano Letters, 4(2), 377 (2004).
[14]S. Roy, and B. P. Pandey, Physics of Plasmas, 9(9), 4052 (2002).
[15]J. P. Boeuf, L. C. Pitchford, Physical Review E, 51(2), 1376 (1995).
[16]M. Lieberman, A. J. Lichtenberg, Principles of plasma discharges and material processing, John Wiley and Sons, Inc., 1994.
[17]Y. P. Raizer, M. N. Shneider and N. A. Yatsenko, Radio-frequency discharges, CRC Press, London, 1995.